Desalination and Water Treatment
www.deswater.com
doi: 10.1080/19443994.2014.961558

56 (2015) 2464–2476
November

Taylor & Francis
Taylor & Francis Group

Optimization of fluoride adsorption onto a sonochemically synthesized nano-MgO/γ-Al_2O_3 composite adsorbent through applying the L_{16} Taguchi orthogonal design

Mahdi Nazari[a], Rouein Halladj[b,*]

[a]*Department of Petrochemical Engineering, Amirkabir University of Technology (Tehran Polytechnic), Mahshahr Campus, P.O. Box 415, Mahshahr, Iran, Tel. +986522622064; email: mahdi_nazari80@yahoo.com (M. Nazari)*
[b]*Department of Chemical Engineering, Amirkabir University of Technology (Tehran Polytechnic), P.O. Box 15875-4413, Hafez Ave., Tehran, Iran, Tel. +98 2164543168; email: halladj@aut.ac.ir (R. Halladj)*

Received 20 December 2013; Accepted 27 August 2014

ABSTRACT

Here in this work an effort has been made to *in situ* dope γ-Al_2O_3 as substrate with MgO nanoparticles through applying wet impregnation followed by sonochemical synthesis methods. The as-synthesized alumina supported nano-magnesia particles (4–30 nm) were evaluated as a new defluoridating agent upon operating conditions such as pH, initial concentration, contact time, temperature and sorbent dose. The L_{16} Taguchi statistical approach was implemented to optimize these operating conditions. The adsorbents were also characterized using the Fourier transform infrared spectroscopy, high resolution scanning electron microscope, X-ray diffraction and X-ray analysis methods. Under optimum conditions of pH 6.00 ± 0.30, initial concentration of 0.05 kg/m^3, dose of 0.70 kg/m^3, contact time of 8400 s and temperature of 298 K, the fluoride removal efficiency was up to 97%. Results of the ANOVA revealed that the most influential factor on the removal efficiency of nanoadsorbent would be the initial concentration of F^- ions followed by solution pH with 31 and 22% contribution, respectively. Moreover, contribution of experimental errors (noise factor) which is actually insignificant (0.06%) and *F*-ratios confirms the accuracy of the obtained results.

Keywords: Defluoridation; Sonochemical; Nanoadsorbent; Magnesium oxide; Taguchi approach; ANOVA

1. Introduction

The World Health Organization (WHO) has classified F^- as one of the contaminants of water and regulated the maximum contamination limits of fluoride to 1.0 mg/L for drinking water and 10.0 mg/L for industrial discharge [1]. Therefore, finding a solution to treat water and wastewater containing excess fluoride concentrations is so important. Among the various defluoridation techniques [2–4], adsorption is the most promising one due to ease of operation and maintenance, lower cost and being relatively more environment friendly process that eventually addresses many of local resources and constraints [5–7]. In the past 10 years, various alumina-based adsorbents have been employed to lower the fluoride level of aqueous

*Corresponding author.

systems [8–10]. Nevertheless, the main disadvantages of alumina are its slow rate of adsorption, residual aluminium and soluble aluminium fluoride complexes, the formation of bulky sludge after the treatment of large amounts of water and narrow available pH range which is typically below than 7.0 [1,11,12]. Recently, considerable amounts of work have been devoted to conquer these limitations by incorporating various types of alkaline and alkaline earth metal oxides into the different adsorptive materials. Magnesia is one of these promoters [13–15]. However, magnesia is only available as fine powder, and using of metal oxide sorbent in powder form has practical limitations [16,17]. In this regard, different composite materials, such as magnesia-amended activated alumina granules [8], magnesium-doped nano-ferrihydrite [16], magnesium-incorporated bentonite clay [18], magnesia-amended silicon dioxide [17], magnesia/chitosan biocomposite [19] and magnesia-loaded fly ash cenospheres [20], have been synthesized and evaluated for F^- removal. Nevertheless, the main drawbacks of these wet chemistry approaches are high cost demands, time consuming and their difficulties to control the morphology of synthesized particles especially when the scale of formed crystals goes down to nanometers. Thus, it was thought desirable to use a new ultrasound-driven synthetic route to modify the surface structure of γ-Al_2O_3 through deposition of sonochemically prepared magnesia nanoparticles on that [21]. Despite the aforesaid methods, this method is very simple, fast and does not need any complicated facilities. The sonochemical method involves radical reactions and/or thermal reactions which originate from the extremely high temperature and pressures generated in the cavitation bubbles [21–23]. Recently, Song et al. [23] and Alavi and Morsali [24] have successfully synthesized magnesium hydroxide (10–17 nm) and magnesia (40–90 nm) nanoparticles with the aid of ultrasonic irradiation.

By thorough literature survey, we found that very few reports are available regarding the sonochemical doping of gamma alumina substrate within an organic phase by nanoscaled magnesium oxide particles to form corresponding nanocomposites [25,26]. Herein, mesoporous high-surface area activated alumina was sonochemically impregnated with MgO nanoparticles and used as a nanocomposite adsorbent in the defluoridation process of aqueous media. The crystalline features, elemental constituents, surface functional groups, particle size and morphology of the resulting adsorbents were characterized by the X-ray diffraction (XRD), X-ray analysis (EDAX), FTIR and high resolution scanning electron microscope (HR-SEM) methods.

The combined effects of solution pH, temperature, dose of adsorbent, contact time and initial fluoride ions concentration on the fluoride uptake efficiency of adsorbent have been statistically investigated by the Taguchi orthogonal array method. Experiments using Taguchi method allow several effects of factors to be simultaneously determined effectively and efficiently. By applying this technique, one can significantly reduce the time required for experimental investigation [27]. More important, the application of statistical experimental design techniques in development stages of adsorption processes can result in improved product yields, reduced process variability, closer confirmation of the output response to nominal and target requirements and reduced development time [28].

2. Design of experiments

The technique of defining and investigating all the possible conditions in an experiment involving multiple factors is known as the design of experiments [29]. To determine the best set of parameters among the effective factors by reducing the number of experiments, the Taguchi method has been chosen. Accordingly, an analysis of the signal-to-noise (S/N) ratio is needed to evaluate the experimental results. Usually, three types of S/N ratio analysis are applicable: (1) lower is better, (2) nominal is better and (3) higher is better [30]:

$$S/N = -10\ \log\left(\frac{\sum_{i=1}^{n}\frac{1}{y_i^2}}{n}\right) \quad (1)$$

where n is the numbers of trials under the same operating conditions and y is the response variable, i.e. fluoride removal efficiency.

3. Experimental

3.1. Materials and methods

All chemicals used in the present study were of analytical reagent grade. A stock solution of 1,000 mg/L fluoride was prepared by dissolving appropriate amounts of sodium fluoride (Merck, Germany) in Millipore de-ionized (Milli-Q 18.2 MΩ cm at 25˚C) water and the entire standard and fluoride-spiked solutions for removal experiments and analyses were prepared by appropriate dilution from the freshly prepared stock solution.

Magnesium nitrate ($Mg(NO_3)_2.6H_2O$, Merck, Germany), ethanol (Merck, Germany) and ammonia (24 wt.% aqueous solution) were used in all the

experiments. The γ-Al_2O_3 used in this study was obtained through dehydration and heat treatment of a well crystalline synthetic boehmite (γ-AlOOH, CERA hydrate) precursor upon a predefined calcination programme. Some of the physicochemical properties of the derived γ-Al_2O_3 are given in Table 1. The dried γ-Al_2O_3 was sieved, and fine powder (mesh < 100 μm) of Al_2O_3 was used as a host for the experiments.

3.2. Preparation of magnesium oxide/alumina nanocomposites

The synthesized fine powder of γ-Al_2O_3 and an aqueous solution of magnesium nitrate with predetermined concentration (5×10^{-4} kg in 1×10^{-4} m^3 of Millipore de-ionized water) and isopropanol (0.05 M) were taken into contact in a 2.50×10^{-4} m^3 round-bottomed flask for 3,600 s with continuous stirring by a Heidolph magnetic stirrer at 150 rpm at room temperature. The argon gas was allowed to bubble through the prepared slurry at a rate of 0.013×10^{-4} m^3/s, before and during irradiation, by an immersed sparger in order to expel dissolved oxygen and to decrease cavitations threshold.

The applied recipe for ultrasound irradiation of as-prepared mixture has been reported elsewhere [23,24,31]. Ultrasonic irradiation was produced by an ultrasound generator UP200H (Hielscher, 24 kHz, 80% pulse ratio, 600 W/cm^2, Germany) with a titanium sonotrode having a tip diameter of 0.007 m. The preliminary experiments revealed that at least one hour is required to complete the reduction and insertion of Mg^{2+} within γ-Al_2O_3 porous host under the conditions used. During sonication, ammonia solution was added dropwise into the reaction slurry which was maintained at a constant cooling bath temperature of 293 K. Finally, the resulted fine precipitate was centrifugally separated from the solution, washed thoroughly with plenty of water and ethanol to assure that the wash out is free from any nitrate ions. Then dried and aged in vacuum oven at 393 K overnight and calcined under He (g) atmosphere at 923 K for 21,600 s to get magnesia nanoparticles from thus synthesized magnesium hydroxide nanostructures through proposed mechanism shown in Fig. 1.

Nanometer-sized MgO particles were also obtained with the same above-mentioned recipe, except that the annealed alumina was not present in the reaction vessel during sonication.

Table 1
Characteristics and chemical composition of boehmite-derived γ-Al_2O_3

Item	Value
Substances extractable by water	<0.5 wt.%
Specific surface area (BET)	190 m^2/gr.
Loss on ignition (1,000°C, 2 h)	1.0 wt.%
Pore volume	0.37 (cm^3/gr.)
Bulk density	950 gr./lit.
Components (wt.%)	Al_2O_3 (99.81)
	SiO_2 (0.04)
	Fe_2O_3 (0.04)
	Na_2O (0.11)

3.3. Characterization of materials

The XRD patterns of the samples were recorded by Philips diffractometer with a copper anode and step sizes of 0.04° and 0.08° in order to identify the crystalline phases of the samples. The obtained patterns were compared with the standards compiled by Joint Committee on Diffraction Pattern and Standards (JCDPS). Examination of samples with HR-SEM with Philips-CM120 model operating at 200 kV and fitted with an energy dispersive EDAX allows a qualitative interpretation of surface morphologies and detection of elements in the as-prepared and F^- loaded materials and further confirms the capturing of targeted fluoride ions within the adsorbent. FTIR spectra of the samples were collected using a PerkinElmer model: Spectrume GX FTIR spectrometer (USA, 2005) in the wavelength range of 4,000–400 cm^{-1} to confirm the formation of expected functional groups. Prior to each analysis, 0.20×10^{-4} kg of the sample was out-gassed at 393 K for 36,000 s under flowing of nitrogen. The pH measurements were done by a Metrohm pH- meter (Model No. E-632, Switzerland). The pH value of zero point charge (pH_{ZPC}) of adsorbent particles was determined through a pH drift method [2].

3.4. Evaluation of adsorbent performance

In order to study the performance of synthesized nanocomposite adsorbent upon batch mode of fluoride adsorption process, a series of 2.50×10^{-4} m^3 Erlenmeyer flasks containing a predetermined mass of sorbent in 100 mL of NaF-spiked solution with a known initial concentration were kept in a Heidolph magnetic stirrer with continuous stirring at 150 rpm, a constant pH at room temperature (298 K) for specified adsorption time intervals, upon which samples were withdrawn to determine the concentration of remained F^- ions. Adjusting the initial pH of the solution is done using 0.01 N HCl or 0.01 N NaOH solutions. After equilibration, the supernatants were

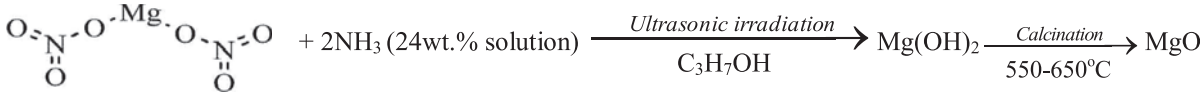

Fig. 1. Mechanism of formation of $Mg(OH)_2$ and MgO through applying ultrasonic field.

centrifugally separated and analyzed for determining residual fluoride concentration by a UV–visible spectrophotometer (Hitachi DR/4000U, Japan) at 570 nm as λ_{max} and as per SPADNS procedure which is described elsewhere [8,32]. We carried out all the other adsorption tests as per designed experimental L_{16} orthogonal array layout. Each trial was repeated two times on two different synthesized nanocomposite samples, and the average value of these measurements was reported for each sample under the same conditions at different times to observe the effects of noise (uncontrollable) sources in the process and to obtain reproducible results with an error of less than 3%.

The clear liquid filtrate was also analyzed by inductively coupled plasma-atomic emission spectroscopy (ICP-AES, Model OPTIMA 4100DV) to detect any trace amounts of leached magnesium from the synthetic adsorbent.

The removal percentage of F^- ($R\%$) and adsorption capacity q_e (mg/g) of adsorbent were calculated using Eqs. (2) and (3), respectively [33]:

$$\% \text{ Removal} = \frac{C_0 - C_e}{C_0} \times 100 \quad (2)$$

$$q_e = (C_0 - C_e) \times \frac{V}{m} \quad (3)$$

The C_0 and C_t are the initial and time dependent final fluoride concentrations (mg/l) in solution, C_e is the concentration of remaining fluoride ions at equilibrium, V is the sorbent free solution volume (l) and m is the sorbent mass (g).

3.5. Scheme of statistically designed experiments

According to literature review, five controllable factors, including agitation time, initial concentration, dose, temperature and pH, all in four levels were selected to be considered in the experiments. Factors and their levels are given in Table 2. The orthogonal array Taguchi L_{16} experimental layout in terms of above-mentioned factors and levels comprising 16 runs with two replicates for each is shown in Table 3. Each row of the orthogonal array represents a run, that is, a specific set of factor levels to be tested. Taguchi suggests analyzing of variations using an appropriately chosen signal-to-noise ratio. In this study, the percentage removal of fluoride ($R\%$) was considered as a measured response. Because the goal in this study is to maximize the response, i.e. the higher removal efficiency, the design belongs to so-called "higher-is-better" type [34].

4. Results and discussion

4.1. Characterization of the adsorbents

4.1.1. XRD patterns

The XRD patterns of the γ-Al_2O_3, pristine MgO and MgO/γ-Al_2O_3 samples prepared by the sonochemical method have been shown in Fig. 2(a–c), respectively. As depicted in Fig. 2(a), for γ-Al_2O_3, there are sharp diffraction peaks of gamma alumina which mainly appeared in $2\theta \approx 32^\circ$, 37.8°, 46° and 67°. In the case of magnesia, Fig. 2(b), the appearance of narrow diffraction peaks of pure Periclase cubic MgO phase mainly situated at d-spacing of 2.433, 2.105 and 1.489 Å corresponding to 2θ of 36.938, 42.932 and 62.332°, respectively, clearly indicates superior crystalline structure of sample which can be assigned to applied synthesis method. Moreover, there was neither any sign of undue agglomeration nor impurity in the sample. As shown in Fig. 2(c), the main crystal phases of the XRD pattern of nano-MgO/γ-Al_2O_3 reveal the formation of hexagonal and face-centred cubic phase of magnesium oxide, measured at $2\theta =$ 43°, 62.3°, 64.58° and 77.54° which match well with the data in JCPDS file No. 45-0946 for fcc MgO particles in the presence of γ-Al_2O_3. By the way, no XRD reflections arising from any impurities, such as $Mg(OH)_2$, were observed. The average grain size of the MgO nanocrystals was estimated using the well-known Debye-Scherer formula, $D = 0.9\lambda/\beta\cos\theta$, where D is the average crystallite size, λ is the X-ray wavelength (0.15405 nm) θ and β are the diffraction angle and full-width line broadening at half maximum of an observed peak, respectively [23,24]. The mean crystallite dimensions were evaluated to lie between 4 and 30 nm in diameter. Fairly same observations were previously reported by other authors, and well-crystallized magnesia nanoparticles were obtained with the size of 72 and 20–27 nm, respectively [23–25].

Table 2
Selected factors and their levels

Factor	Description	L1	L2	L3	L4
A	Agitation time (sec)	600	1,800	7,200	14,400
B	Concentration (kg/m^3)	0.005	0.010	0.015	0.020
C	Dose (kg/m^3)	0.100	0.300	0.500	0.700
D	Temperature (K)	293	298	303	308
E	pH	2	4	6	8

Table 3
The layout of the Taguchi L_{16} orthogonal array

Experiment No. 1	A	B	C	D	E
1	600	0.005	0.100	293	2
2	600	0.010	0.300	298	4
3	600	0.015	0.500	303	6
4	600	0.020	0.700	308	8
5	1,800	0.005	0.300	303	8
6	1,800	0.010	0.100	308	6
7	1,800	0.015	0.700	293	4
8	1,800	0.020	0.500	298	2
9	7,200	0.005	0.500	308	4
10	7,200	0.010	0.700	303	2
11	7,200	0.015	0.100	298	8
12	7,200	0.020	0.300	293	6
13	14,400	0.005	0.700	298	6
14	14,400	0.010	0.500	293	8
15	14,400	0.015	0.300	308	2
16	14,400	0.020	0.100	303	4

After the sorption of fluoride ions on as-prepared nanocomposite adsorbent, the peaks pertained to the alumina and magnesia showed no remarkable variations (not shown). Indeed, doping of fluoride ions onto the alumina seldom alters the crystalline nature of the constituent adsorbent [6].

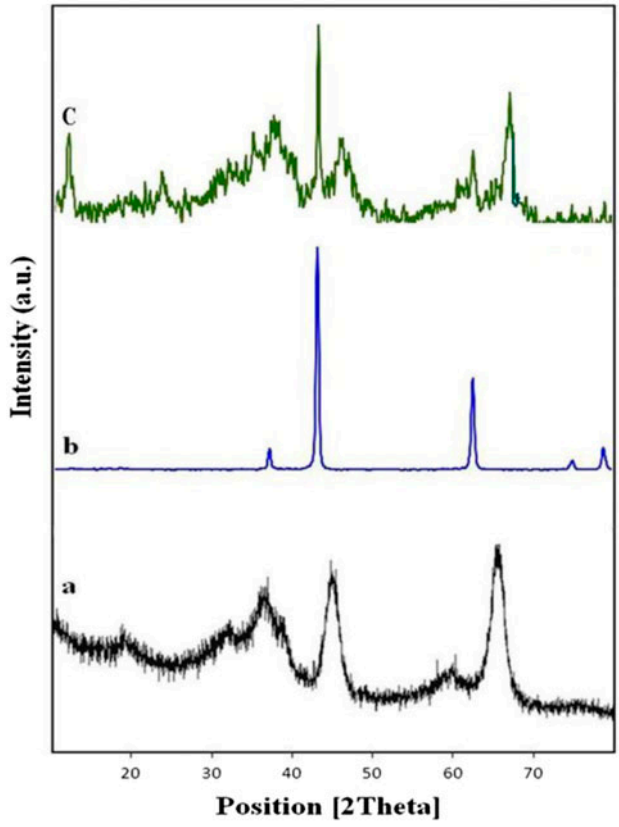

Fig. 2. XRD patterns of the (a) γ-Al_2O_3 (b) ultrasonically synthesized nano-MgO particles and (c) ultrasonically synthesized nano-MgO/γ-Al_2O_3 composite.

4.1.2. HR-SEM images

Fig. 3 shows well-ordered appearance, small and semi-spherical MgO particles in the form of HR-SEM images of the pristine magnesia particles derived upon ultrasound field. Relatively, regular morphology and good dispersion with no serious agglomeration in particles imply that making use of ultrasonic irradiation may well restrict undue crystal growth of MgO particles during the synthesis process. As it is evident from Fig. 4, the ultrasound assisted synthesized MgO particles coated on γ-Al_2O_3 are uniformly distributed in the sample with a layered berry-like surface appearance without any serious agglomeration that can be easily distinguished from γ-Al_2O_3 by their more bright shadow. The average crystal sizes of nanoparticles, mainly composed of very fine agglomerated primary particles, were ca. 13–25 nm in diameter with a regular spherical shape. It seems that the above-discussed morphological features of the synthesized nanomaterials are close to the observations of Nagappa and Chandrappa [35] and Alavi and Morsali [24].

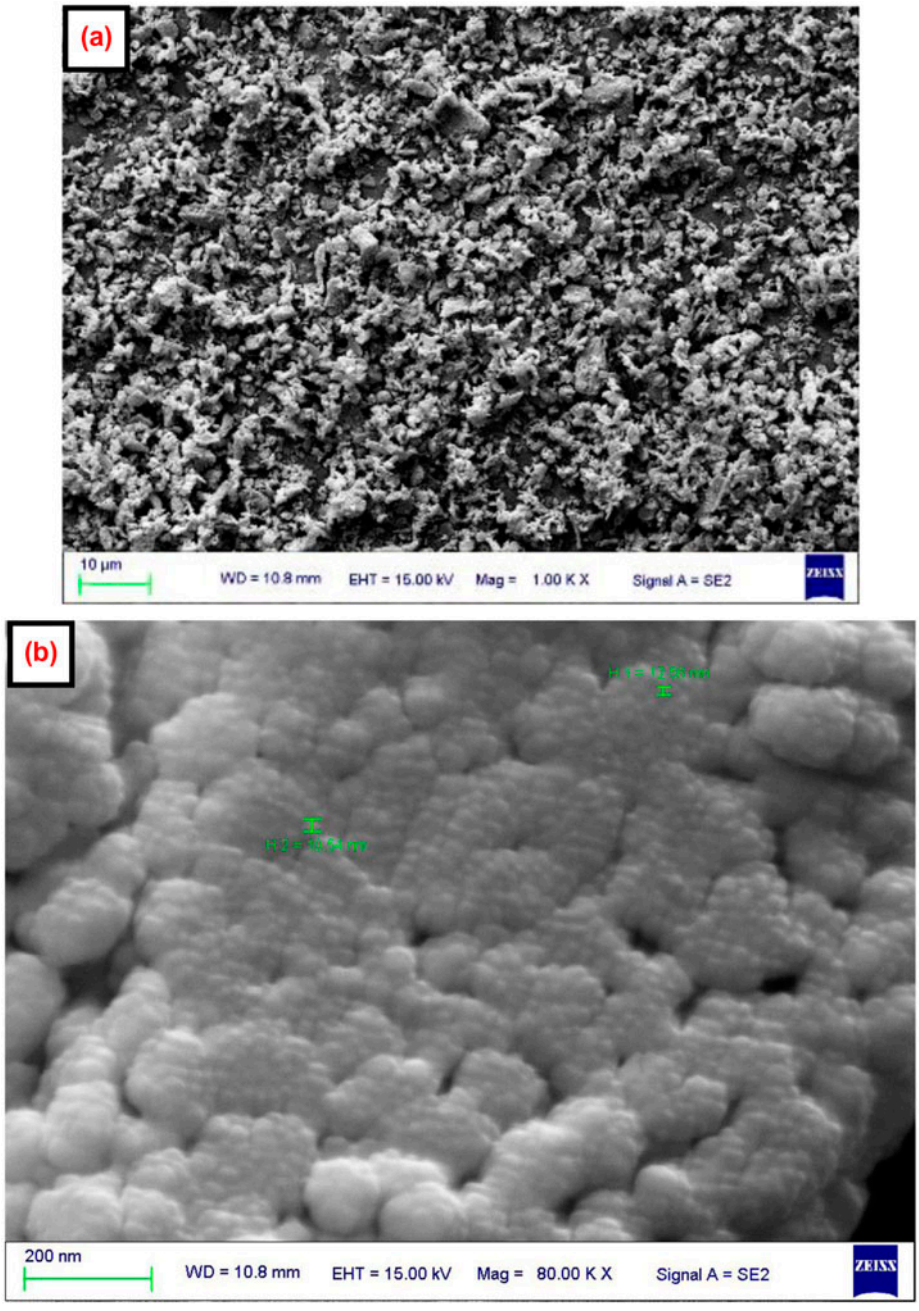

Fig. 3. The HR-SEM images of sonochemically obtained magnesia (MgO) nanoparticles at different magnifications (the scale bars in descending orders: 10 µm, 200 nm).

4.1.3. Elemental analysis by EDAX

The elemental constituents of the as-prepared MgO nanostructures and MgO/γ-Al_2O_3 nanocomposite (theoretically contained 2.5 wt.% of magnesium as magnesia) determined by energy dispersive EDAX spectra are shown in Fig. 5.

Expectedly, only Mg, O and Al elements are present into the sonochemically deposited magnesia nanoparticles on γ-alumina, as shown in Fig. 5(b), which further confirms the applicability of acoustic cavitation route to *in situ* prepare nanostructured materials. The wt.% of Al, O and Mg elements in the magnesia/alumina nanocomposite, estimated from its corresponding EDAX, were found to be ~61.5, 36.4 and 2.4%, respectively, which are close to molar ratio of magnesium nitrate to alumina in the precursor

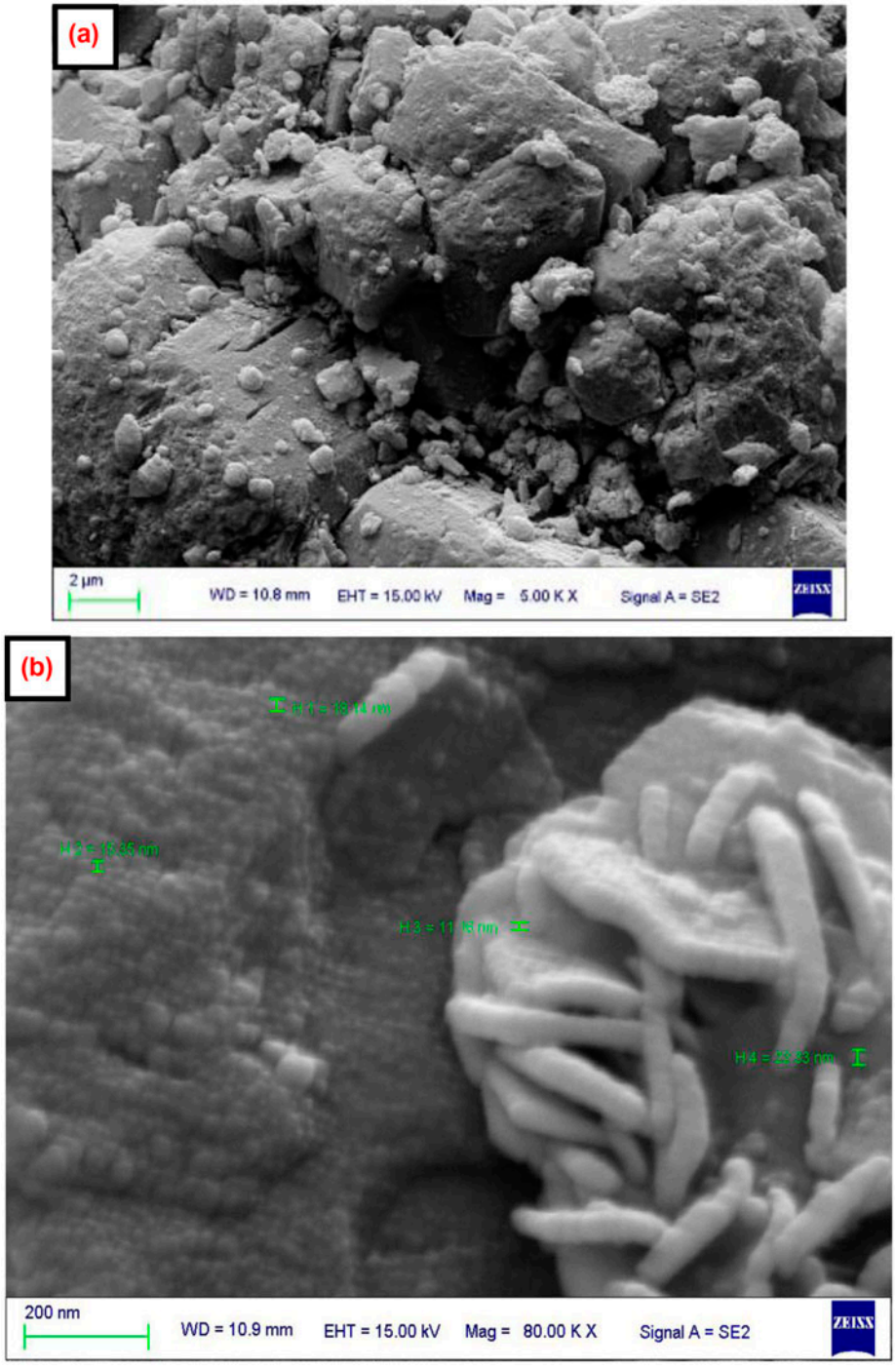

Fig. 4. The HR-SEM images of sonochemically obtained MgO/γ-Al_2O_3 composites at different magnifications (the scale bars in descending orders: 10 µm, 2 µm and 200 nm).

solution. For the pristine MgO sample, as shown in Fig. 5(a), there were two peaks ascertain to Mg and O as the only elements present in the sample with ~76 and 24 wt.%, respectively. No impurity phases were observed in the samples.

4.1.4. FT-IR spectra

The FT-IR spectra of nanocrystalline MgO and nano-magnesia/γ-Al_2O_3 adsorbents (before and after the adsorption tests) have been shown in Fig. 6. In the

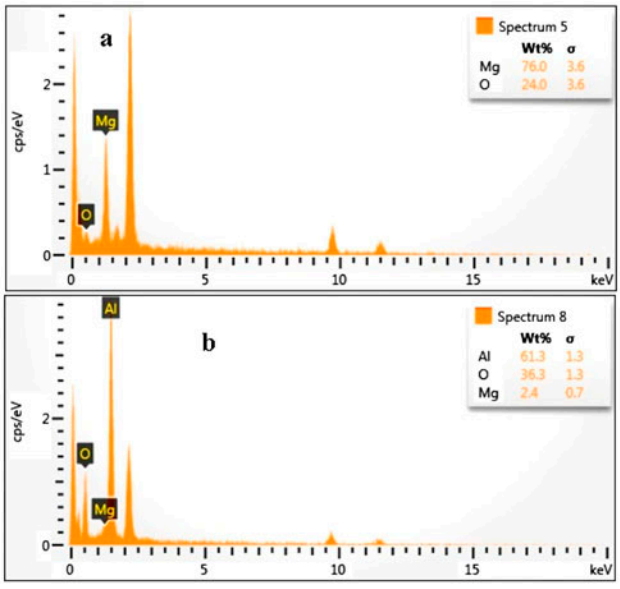

Fig. 5. The energy dispersive analysis of X-ray (EDAX) of the (a) pristine nanostructured MgO (b) nanometer size MgO loaded γ-Al_2O_3 composites (2.5 wt.% loading).

FT-IR spectra of the pristine MgO, characteristic peak of O–H band stretch at the range of 3,695–3,700.37 cm^{-1} was observed in Fig. 6(a). The broad peaks at around 3,452 cm^{-1} and 1,638 cm^{-1} could be ascertained to the stretching vibrations of hydroxyl groups and molecular water, respectively. A twin peak in the finger print region explained the metal-oxygen stretching vibration [36].

Upon deposition of magnesium oxide nanoparticles onto the γ-Al_2O_3 structure, no drastic structural modifications would occur in γ-Al_2O_3 as shown in Fig. 6(b). Moreover, the major infrared absorption peaks at around 3,400–3,440 cm^{-1} and 1,640–1,650 cm^{-1} can be attributed to the stretching and bending vibrations of hydroxyl groups and water molecules, respectively. The peak shifting to 3,400 cm^{-1} (lower frequency) and reduction (slight broadening) in the intensity of bands ascertain to –OH, as depicted in Fig. 6(c) for the spectra of fluoride-contacted magnesium-incorporated alumina adsorbent compared with fresh one, can be considered as evidence for the involvement of –OH bonds in the interactions with fluoride ions through the formation of O–H···F hydrogen bonding [19].

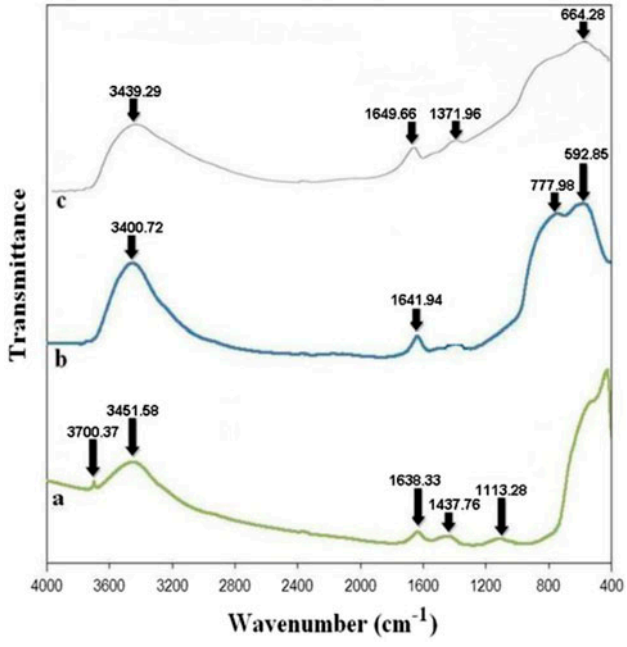

Fig. 6. FT-IR spectra of (a) pristine MgO (b) MgO/γ-Al_2O_3 nanocomposite (before F^- sorption) and (c) MgO/γ-Al_2O_3 nanocomposite (after F^- sorption).

4.2. Preliminary evaluation of adsorbent performance

The time-dependent performance of untreated γ-Al_2O_3 and nano-MgO/γ-Al_2O_3 adsorbents in terms of the variation of residual F^- ions concentration in the test solution against contact time, under identical set of conditions as 5×10^{-4} kg adsorbent in 1×10^{-4} m^3 of aqueous solution initially contained 5, 10, 15 and 20 mg/l of F^-, pH 6.0 ± 0.3, stirring speed of 150 rpm at 308 K, was examined. The obtained results are depicted in Fig. 7, which clearly reveal an improved fluoride uptake capacity onto the MgO-doped γ-Al_2O_3 adsorbent as compared to that of unmodified γ-Al_2O_3 for the all examined initial fluoride concentrations. It can be

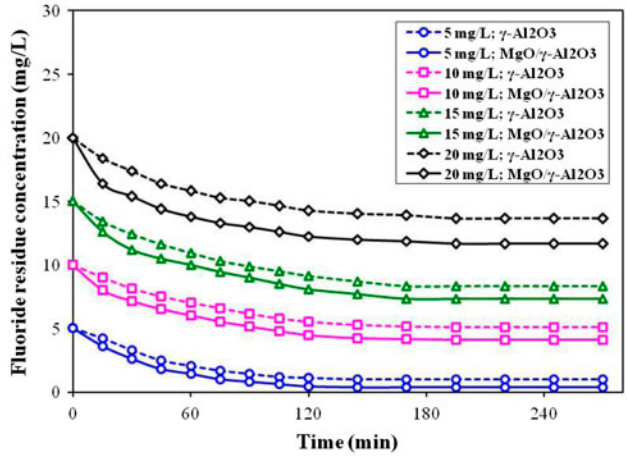

Fig. 7. Fluoride depletion rate as a function of initial concentration for γ-Al_2O_3 and nano-MgO/γ-Al_2O_3 composite (pH 6.0 ± 0.3, dose = 0.5 kg/m^3, temperature = 308 K).

Table 4
Calculated S/N ratio and removal efficiencies as per the Taguchi L_{16} OA layout

Experiment No.	$(R\%)_1$	$(R\%)_2$	Average $R\%$	S/N
1	28.00	28.30	28.15	28.98
2	31.00	28.74	29.87	29.48
3	63.00	63.01	63.01	35.98
4	48.40	46.50	47.45	33.51
5	65.50	65.35	65.43	36.31
6	55.50	55.45	55.48	34.88
7	32.50	32.49	32.50	30.23
8	26.60	26.00	26.30	28.39
9	78.50	78.35	78.43	37.88
10	68.50	66.30	67.40	36.56
11	51.00	51.10	51.05	34.15
12	41.00	41.10	41.05	32.26
13	95.75	95.75	**95.75**	**39.62**[a]
14	68.00	68.98	68.49	36.71
15	48.50	48.00	48.25	33.66
16	32.70	32.60	32.65	30.27

Note: The bold value (95.75) refers to max. calculated average fluoride removal efficiency among the sixteen experimental runs.
[a]The maximum calculated S/N ratio among the sixteen experimental runs.

observed from Fig. 7 that the adsorbent dosage of 0.5 kg/m^3 was sufficient to decrease the initial level of fluoride contamination to near safe limit. It is also obvious that the kinetics of fluoride sorption onto the synthesized nanosorbent is faster than γ-Al_2O_3, especially during the first 60 min of adsorption. Nevertheless, the rate of adsorption was negligible after 140 min of experiment at all cases, and thereafter the residual fluoride concentrations gradually reached a plateau which corresponds to pseudo-equilibrium conditions. As the equilibrium time is not totally affected by ions concentration, we considered the 8400 s as the minimum required contact time to have a maximum fluoride adsorption by the adsorbents. The maximum removal percentage of F^- ions on the nanocomposite adsorbent for $C_0 = 0.005$ kg/m^3 was more than 80.0% which is comparable to that attained on γ-Al_2O_3, i.e. 76.80%.

4.3. Statistical analysis of adsorption data

The fluoride removal efficiency of MgO/γ-Al_2O_3 nanocomposite adsorbent for indicated runs in Table 3 was measured, and results are given in Table 4. Also in this Table, the S/N ratio of each run calculated from Eq. (1) is given. Now from obtained data, as shown in Table 4, the mean of S/N ratio and the mean response (removal efficiency) variable for each factor at a certain level can be determined. The results are summarized in Tables 5 and 6, respectively. The mean of S/N ratio for each level of a certain factor shows the effect of that level of factor on the response, independently. It is calculated by averaging the S/N ratio values of all the experiments where the level of that factor has been used. In Table 5, the boldfaces refer to the maximum value of the mean of the S/N ratios of a certain factor among four levels. Besides, the difference between levels in Table 5 also shows which factor is more significant. The most significant factors that affect fluoride removal are ranked as follows: initial concentration > pH > contact time > temperature > adsorbent dose.

Based on the given data, as shown in Table 6, the mean response diagrams can be constructed with respect to five aforementioned controllable factors. The results are shown in Figs. 8–12. According to these figures, increasing the contact time, adsorbent dose, temperature and pH of solution increases the removal efficiency of nanosorbent.

Herein, the analysis of variance (ANOVA) statistical approach was applied in order to ascertain which factor will affect the response variable more significantly [37]. The ANOVA (Table 7) will compute such quantities as degrees of freedom (DF), sequential sums of squares (Seq SS), adjusted sums of squares (Adj SS), variance (V), *F*-ratio and relative percentage contribution (*P*%) among the factors [30]. The "*F*-ratio" is a well-known statistical parameter of the ANOVA table and represents the ratio of factor variance on error variance. *F*-test indicates which of the examined process parameters have a significant effect in obtaining

Table 5
Calculated mean of S/N ratio for data obtained from fluoride removal experiments

Level	Time	Concentration	Dose	Temperature	pH
1	32.00	**35.70**	32.08	32.05	31.91
2	32.46	34.42	32.94	32.92	31.98
3	**35.22**	33.51	34.75	34.79	**35.69**
4	35.07	31.12	**34.98**	**34.99**	35.18
Difference	3.22	4.59	2.91	2.94	3.78
Rank	3	1	5	4	2

Note: The bold values at each column of this table refer to maximum calculated S/N ratio according to the "larger is better" criterion.

Table 6
Calculated mean of response (removal efficiency) for each factor at its corresponding four levels

Level	Time	Concentration	Dose	Temperature	pH
1	42.12	**66.94**	41.83	42.55	42.53
2	44.92	55.31	46.15	50.74	43.36
3	59.48	48.70	59.06	57.12	**63.82**
4	**61.29**	36.86	**60.77**	**57.40**	58.10
Difference	19.17	30.08	18.94	14.85	21.30
Rank	3	1	4	5	2

Note: The bold values at each column of this table refer to maximum calculated mean of response (fluoride removal efficiency).

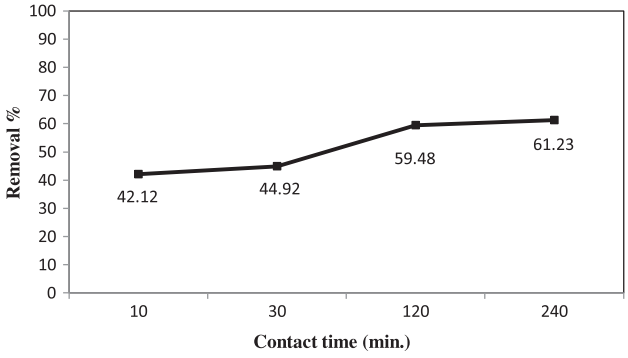

Fig. 8. Main effect plot of agitation time on the mean of response (fluoride removal efficiency).

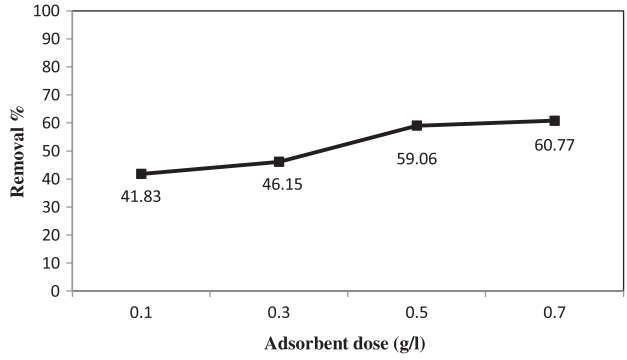

Fig. 10. Main effect plot of adsorbent dosage on the mean of response (fluoride removal efficiency).

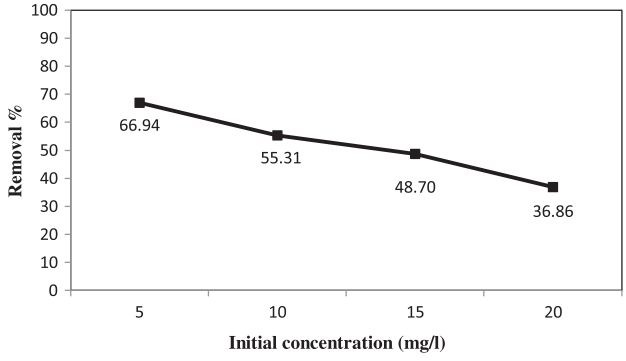

Fig. 9. Main effect plot of initial concentration on the mean of response (fluoride removal efficiency).

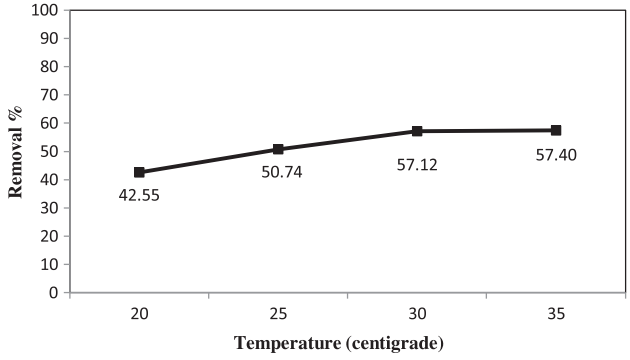

Fig. 11. Main effect plot of solution temperature on the mean of response (fluoride removal efficiency).

the maximum removal efficiency [38]. The optimal combination of process variables can be determined together with the performance characteristics of adsorbent and ANOVA analyses. As it is shown in Fig. 13, the most influential factor on removal efficiency is the initial concentration of F^- ions with 31.25% contribution, followed by pH (22.50%), contact time and adsorbent dosage. Moreover, the values of *F*-ratio parameter for selected factors confirm again the mentioned order for contribution of them on the response variable. In this regard, the temperature of solution does not significantly influence the response variable as gets the lowest *F*-ratio among the other factors (Table 7).

Consequently, the optimum conditions for adsorptive removal of fluoride ions from aqueous solution on the basis of maximizing the removal efficiency and consequently the S/N ratio can be concluded as: the agitation time of 14,400 s (A4), the initial concentration of 0.005 kg/m^3 (B1), the adsorbent dosage of

Table 7
ANOVA table for F^- ions removal process

Source	df	SS	Variance	STDV	*F*	*P*%
Contact time (sec)	3	2,319.069	773.023	27.803	1,617.234	19.109
Concentration (kg/m^3)	3	3,792.812	1,264.271	35.557	2,644.970	31.252
Dose (kg/m^3)	3	2,115.065	705.022	26.552	1,474.970	17.428
Temperature (K)	3	1,170.560	390.187	19.753	816.306	9.645
pH	3	2,731.074	910.358	30.172	1,904.552	22.503
Error	16	7.648	0.478			0.060
Total	31	1,2136.228				100

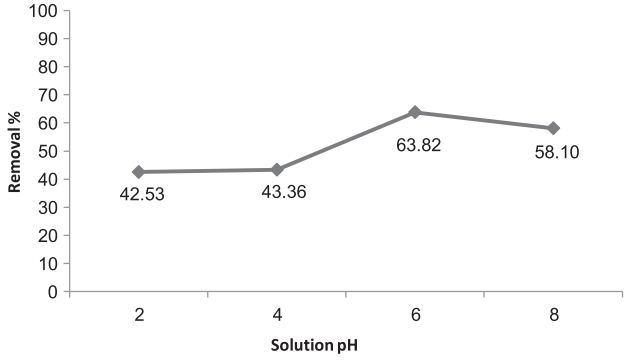

Fig. 12. Main effect plot of solution pH on the mean of response (fluoride removal efficiency).

0.700 kg/m^3 (C4), the temperature is 298 K (D2) and the pH is 6 (E3). These factor settings represent the operating conditions of run No. 13 with the largest values of removal efficiency and S/N ratio among all (Table 4).

5. Conclusions

Systematic researches were conducted on boehmite-derived γ-Al_2O_3 coated with sonochemically prepared electropositive nano-magnesia particles to obtain information about the defluoridation capacity and physicochemical characteristic features of this nanocomposite material. Nanocrytallinity of the prepared samples was assessed through HR-SEM and XRD techniques from which the estimated size of magnesia nanoparticles, reside onto the alumina structure, were in the range of 5–25 nm range. The results showed that this material could be able to decrease fluoride concentration from aqueous solutions at a higher rate with considerably more capacity, as compared to the conventional γ-Al_2O_3 adsorbent. Moreover, using the L_{16} Taguchi orthogonal array method, the optimum operating conditions for abating the fluoride ions from aqueous solutions were obtained as follows: pH of 6.0 ± 0.3, dose of 0.7 kg/m^3, temperature of 298 K, initial concentration of 0.005 kg/m^3 and contact time of 14,400 s to get more

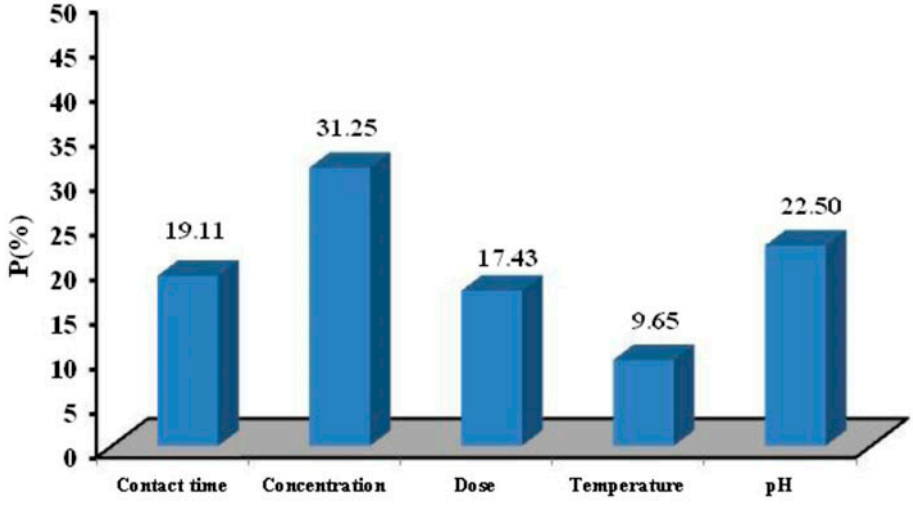

Fig. 13. Contribution percentage of selected controllable factors on removal efficiency of nano-MgO/γ-Al_2O_3 adsorbent.

than 97% removal efficiency by nanosorbent. Results of the ANOVA table revealed that initial concentration followed by pH was the most influential factor on the removal efficiency of nano-MgO/γ-Al_2O_3 adsorbent with around 31 and 22% of percentage contribution, respectively. The FTIR results provide further evidences for lowering of fluoride concentration through interaction of them with surface –OH groups of the nanosorbent. The results show that the fluoride removal efficiency was slightly affected as a result of the presence of other anions in aqueous solution. However, the decrease of the fluoride adsorption was in order of phosphate > bicarbonate > nitrate > sulphate > chloride. As reviewed, the powdered nanostructured magnesia on γ-Al_2O_3 holds great potential to be used as an effective defluoridation agent in water treatment.

Acknowledgement

The authors would like to express their sincere gratitude to Mr Hamid Sanaeipour (Amirkabir University of Technology, Mahshahr Campus), Mr. Akbar Tangtakabi (R&D Center, BIPC) and Mr. Mahdi Khajeh (Karoon Petrochemicals Co.) for their considerable contributions towards this research.

Nomenclature

- C_0 — initial concentration of fluoride (mg/L)
- C_e — equilibrium concentration of fluoride in the solution (mg/L)
- V — sorbent-free solution volume (L)
- m — sorbent mass (g)
- q_e — amount of fluoride ions adsorbed at equilibrium (mg/g)

References

[1] Y. Tang, X. Guan, T. Sua, N. Gao, J. Wang, Fluoride adsorption onto activated alumina: Modeling the effects of pH and some competing ions, Colloids Surf. A: Physicochem. Eng. Aspects 337 (2009) 33–38.
[2] R. Simons, Trace element removal from ash dam waters by nano-filtration and diffusion dialysis, Desalination 89 (1993) 325–341.
[3] M.G. Sujana, R.S. Thakur, S.B. Rao, Removal of fluoride from aqueous solution by using alum sludge, J. Colloid. Inter. Sci. 206 (1998) 94–101.
[4] S. Meenakshi, N. Viswanathan, Identifying of selective ion-exchange resin for fluoride sorption, J. Colloid. Interface Sci. 308 (2007) 438–450.
[5] H. Kai, S.J. Gang, Z.H. Min, I. Katsutoshi, Removal of fluoride from aqueous solution onto Zr-loaded garlic peel (Zr-GP) particles, Cent. South Univ. Technol. 18 (2011) 1448–1453.
[6] A. Goswami, M.K. Purkait, The defluoridation of water by acidic alumina, Chem. Eng. Res. Des. 90 (2012) 2316–2324.
[7] S. Rengaraj, Y. Kim, C.K. Joo, J. Yi, Removal of copper from aqueous solution by aminated and protonated mesoporous aluminas: Kinetics and equilibrium, J. Colloid. Inter. Sci. 273 (2004) 14–21.
[8] S.M. Maliyekkal, S. Shukla, L. Philip, I.M. Nambi, Enhanced fluoride removal from drinking water by magnesia-amended activated alumina granules, Chem. Eng. J. 140 (2008) 183–192.
[9] S. Ghorai, K.K. Pant, Equilibrium, kinetics and breakthrough studies for adsorption of fluoride on activated alumina, Sep. Purif. Technol. 42 (2005) 265–271.
[10] M.S. Onyango, H. Matsuda, Fluoride Removal from Water Using Adsorption Technique, Fluorine and The Environment, vol. 2, Elsevier B.V., Pessac Cedex, Bordeaux, 2006.
[11] A. Bansiwal, P. Pillewan, R.B. Biniwale, S.S. Rayalu, Copper oxide incorporated mesoporous alumina for defluoridation of drinking water, Microporous Mesoporous Mater. 129 (2010) 54–61.
[12] N. Chen, Z. Zhang, C. Feng, M. Li, D. Zhu, R. Chen, N. Sugiura, An excellent fluoride sorption behavior of ceramic adsorbent, J. Hazard. Mater. 183 (2009) 460–465.
[13] A.C. Zettlemoyer, E.A. Zettlemoyer, W.C. Walker, Active Magnesia. II: Adsorption of fluoride from aqueous solution, J. Am. Chem. Soc. 69 (1947) 1312–1315.
[14] P. Venkateswarlu, D.N. Rao, Investigation on the fluoride removal from water: Rapid removal of fluoride with magnesium oxide, Ind. J. Med. Res. 41 (1953) 473–477.
[15] S.M. Maliyekkal, Anshup, K.R. Antony T. Pradeep, High yield combustion synthesis of nanomagnesia and its application for fluoride removal, Sci. Total Environ. 408 (2010) 2273–2282.
[16] M. Mohapatra, D. Hariprasad, L. Mohapatra, S. Anand, B.K. Mishra, Mg-doped nano ferrihydrite–A new adsorbent for fluoride removal from aqueous solutions, Appl. Surf. Sci. 258 (2012) 4228–4236.
[17] P. Zhu, H. Wang, B. Sun, P. Deng, S. Hou, Y. Yu, Adsorption of fluoride from aqueous solution by magnesia-amended silicon dioxide granules, J. Chem. Tech. Biotech. 84 (2009) 1449–1455.
[18] D. Thakre, S. Rayalu, R. Kawade, S. Meshram, J. Subrt, N. Labhsetwar, Magnesium incorporated bentonite clay for defluoridation of drinking water, J. Hazard. Mater. 180 (2010) 122–130.
[19] C.S. Sundaram, N. Viswanathan, S. Meenakshi, Defluoridation of water using magnesia/chitosan composite, J. Hazard. Mater. 163 (2009) 618–624.
[20] X. Xu, Q. Li, H. Cui, J. Pang, L. Sun, H. An, J. Zhai, Adsorption of fluoride from aqueous solution on magnesia-loaded fly ash cenospheres, Desalination 272 (2011) 233–239.
[21] K.S. Suslick, Ultrasound: Its Chemical, Physical and Biological Effects, VCH, New York, NY, 1988.
[22] A. Gedanken, Using sonochemistry for the fabrication of nanomaterials, Ultrason. Sonochem. 11 (2004) 47–55.
[23] G. Song, S. Ma, G. Tang, X. Wang, Ultrasonic-assisted synthesis of hydrophobic magnesium hydroxide nanoparticles, Colloid. Surf. A: Physicochem. Eng. Aspect. 364 (2010) 99–104.

[24] M.A. Alavi, A. Morsali, Syntheses and characterization of $Mg(OH)_2$ and MgO nanostructures by ultrasonic method, Ultrason. Sonochem. 17 (2010) 441–446.
[25] A. Troia, M. Pavese, F. Geobaldo, Sonochemical preparation of high surface area $MgAl_2O_4$ spinel, Ultrason. Sonochem. 16 (2009) 136–140.
[26] Q. Chang, L. Zhu, Z. Luo, M. Lei, S. Zhang, H. Tang, Sono-assisted preparation of magnesium–aluminum layered double hydroxides and their application for removing fluoride, Ultrason. Sonochem. 18 (2011) 553–561.
[27] V.C. Srivastava, I.D. Mall, I.M. Mishra, Optimization of parameters for adsorption of metal ions onto rice husk ash using Taguchi's experimental design methodology, Chem. Eng. J. 140 (2008) 136–144.
[28] M. Mourabet, A. El Rhilassi, H. El Boujaady, M. Bennani-Ziatni, R. El Hamri, A. Taitai, Removal of fluoride from aqueous solution by adsorption on hydroxyapatite (HAp) using response surface methodology, J. Saudi Chem. Soc. (2012) in press. Available from: http://dx.doi.org/10.1016/j.jscs.2012.03.003.
[29] G. Moradi, J. Ahmadpour, M. Nazari, F. Yaripour, Effects of feed composition and space velocity on direct synthesis of dimethyl ether from syngas, Ind. Eng. Chem. Res. 47 (2008) 7672–7679.
[30] S. Askari, R. Halladj, M. Nazari, Statistical analysis of sonochemical synthesis of SAPO-34 nanocrystals using Taguchi experimental design, Mater. Res. Bull. 48 (2013) 1851–1856.
[31] V.G. Pol, D.N. Srivastava, O. Palchik, V. Palchik, M.A. Slifkin, A.M. Weiss, A. Gedanken, Sonochemical deposition of silver nanoparticles on silica spheres, Langmuir 18 (2002) 3352–3357.
[32] American Public Health Association (APHA), Standard Methods for the Examination of Water and Wastewater, twentieth ed., American Water Work, Washington, DC, 1998.
[33] V. H-Montoya, L.A. Ramirez-Montoya, A. Bonilla-Petriciolet, M.A. Montes-Moran, Optimizing the removal of fluoride from water using new carbons obtained by modification of nut shell with a calcium solution from egg shell, Biochem. Eng. J. 62 (2012) 1–7.
[34] M. Nazari, R. Halladj, Adsorptive removal of fluoride ions from aqueous solution by using sonochemically synthesized nanomagnesia/alumina adsorbents: An experimental and modeling study, J. Taiwan Inst. Chem. Eng. (2014) in press. Available from: http://dx.doi.org/10.1016/j.jtice.2014.05.020.
[35] B. Nagappa, G.T. Chandrappa, Mesoporous nanocrystalline magnesium oxide for environmental remediation, Microporous Mesoporous Mater. 106 (2007) 212–218.
[36] M. Bhaumik, T.Y. Leswifi, A. Maity, V.V. Srinivasu, M.S. Onyango, Removal of fluoride from aqueous solution by polypyrrole/Fe_3O_4 magnetic nanocomposite, J. Hazard. Mater. 186 (2011) 150–159.
[37] G.R. Moradi, M. Nazari, F. Yaripour, Statistical analysis of the performance of a bi-functional catalyst under operating conditions of LPDME process, Chem. Eng. J. 140 (2008) 255–263.
[38] E. Saljoughi, M. Sadrzadeh, T. Mohammadi, Effect of preparation variables on morphology and pure water permeation flux through asymmetric cellulose acetate membranes, J. Mem. Sci. 326 (2009) 627–634.